A zero-voltage conductance peak from weak antilocalization in a Majorana nanowire

Pikulin, D.I.; Dahlhaus, J.P.; Wimmer, M.; Schomerus, H.; Beenakker, C.W.J.

PAPER • OPEN ACCESS

A zero-voltage conductance peak from weak antilocalization in a Majorana nanowire

New Journal of Physics
The open access journal for physics

A zero-voltage conductance peak from weak antilocalization in a Majorana nanowire

D I Pikulin[1,3], J P Dahlhaus[1], M Wimmer[1], H Schomerus[2] and C W J Beenakker[1]

[1] Instituut-Lorentz, Universiteit Leiden, PO Box 9506, 2300 RA Leiden, The Netherlands
[2] Department of Physics, Lancaster University, Lancaster, LA1 4YB, UK
E-mail: pikulin@lorentz.leidenuniv.nl

New Journal of Physics **14** (2012) 125011 (21pp)
Received 27 August 2012
Published 18 December 2012
Online at http://www.njp.org/
doi:10.1088/1367-2630/14/12/125011

Abstract. We show that weak antilocalization by disorder competes with resonant Andreev reflection from a Majorana zero mode to produce a zero-voltage conductance peak of order e^2/h in a superconducting nanowire. The phase conjugation needed for quantum interference to survive a disorder average is provided by particle–hole symmetry—in the absence of time-reversal symmetry and without requiring a topologically nontrivial phase. We identify methods of distinguishing the Majorana resonance from the weak antilocalization effect.

[3] Author to whom any correspondence should be addressed.

Contents

1. Introduction

Weak localization (or antilocalization) is the systematic constructive (or destructive) interference of phase conjugate series of scattering events. In disordered metals it is time-reversal symmetry that provides for phase conjugation of backscattered electrons and protects their interference from averaging out to zero [1, 2]. A magnetic field breaks time-reversal symmetry, changing the disorder-averaged conductance by an amount δG of order e^2/h. The sign of δG distinguishes weak localization ($\delta G < 0$, conductance dip) from weak antilocalization ($\delta G > 0$, conductance peak).

Andreev reflection at a superconductor provides an alternative mechanism for phase conjugation due to particle–hole symmetry. No time-reversal symmetry is needed, so weak (anti)localization can coexist with a magnetic field and is only destroyed by a bias voltage [3, 4]. The resulting zero-bias anomaly in the conductance of a normal-metal–superconductor (NS) junction is obscured in zero magnetic field by the much larger effects of induced superconductivity, which scale with the number of transverse modes N in the junction. These order Ne^2/h effects are suppressed by a magnetic field; only the order e^2/h effect from weak (anti)localization remains [5].

In a superconducting nanowire, there is an altogether different origin of zero-bias anomalies in a magnetic field, namely the midgap state that appears at the NS interface following a topological phase transition [6–8][4]. Resonant Andreev reflection from the zero mode gives a $2e^2/h$ conductance peak at zero voltage [9]. The first reports [10–12] of this signature of a Majorana fermion are generating much excitement [13]. There is an urgent need to understand the effects of disorder in order to determine whether it may produce low-lying resonances that obscure the Majorana resonance [14–18].

These recent developments have motivated us to investigate the interplay of Majorana zero modes and weak (anti)localization. Earlier studies of weak (anti)localization at an NS

[4] Two reviews of the search for Majorana fermions in superconductors are given in [8].

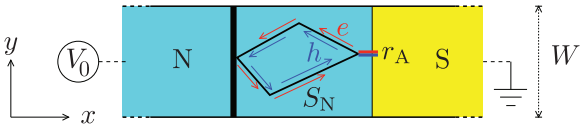

Figure 1. A bias voltage V_0 applied to the normal metal (N) drives a current I into the grounded superconductor (S). Electrons and holes (e, h) are scattered by disorder or a tunnel barrier in N and converted into each other by Andreev reflection at the NS interface, as described by the scattering matrices S_N and r_A. Particle–hole symmetry ensures that the phase shifts accumulated by e and h along a closed trajectory cancel, irrespective of whether time-reversal symmetry is broken or not. Such phase conjugate series of scattering events permit weak (anti)localization to persist in a magnetic field.

junction [3, 4, 19–21] did not consider the possibility of a topologically nontrivial phase with Majorana fermions. Calculations of the local density of states near a zero mode [22–24] address the same physics of midgap quantum interference that we do, but cannot determine the conductance.

This paper consists of two parts. Firstly, in section 2 we give a simple model of a disordered NS interface that allows us to obtain analytical results for δG with and without Majorana zero modes. We then turn in section 3 to a numerical simulation of a Majorana nanowire and compare the conductance peak due to weak antilocalization (in the topologically trivial phase) with that from a Majorana zero mode (in the nontrivial phase). The two effects can appear strikingly similar, but in the concluding section 4 we will discuss several ways in which they may be distinguished.

Before we present our findings, we wish to emphasize that it is not the purpose of this work to diminish the significance of experiments reporting the discovery of Majorana fermions in superconductors. In contrast, we feel that existing [10–12] and forthcoming experiments will gain in significance if possible alternative mechanisms for zero-voltage conductance peaks in a magnetic field are identified and understood, so that they can be ruled out. Weak antilocalization was so far overlooked as one such mechanism.

2. Analytical theory

For the analytical calculation we consider a superconducting wire that supports Q topologically protected zero modes at the interface with a normal metal (see figure 1). The stability of Majorana zero modes depends crucially on the fundamental symmetries of the system [25]. At most a single zero mode is topologically protected if both time-reversal symmetry is broken (by a magnetic field) and spin–rotation symmetry is broken (by spin–orbit coupling), so that only particle–hole symmetry remains. This is called symmetry class D with $Q \in \{0, 1\}$. If the wire is sufficiently narrow (relative to the spin–orbit coupling length), an approximate chiral symmetry [26][5] stabilizes up to N zero modes. (The integer N is the number of propagating

[5] Chiral symmetry of the Hamiltonian is expressed by $H \mapsto -H$ upon exchange $e \leftrightarrow h$ of the electron and hole degrees of freedom. It is broken by spin–orbit coupling of transverse momentum, unlike the more fundamental particle–hole symmetry $H \mapsto -H^*$.

electronic modes through the wire in the normal state, counting both spin and orbital degrees of freedom.) This is called symmetry class BDI with $Q \in \{0, 1, 2, \ldots, N\}$.

2.1. Scattering matrix

We construct the scattering matrix of the NS junction at the Fermi level by assuming a spatial separation of normal scattering in N and Andreev reflection in S. Within the excitation gap there is no transmission through the superconductor. The matrix r_A of Andreev reflection amplitudes from the superconductor is then a $2N \times 2N$ unitary matrix. Mode mixing at the NS interface can be incorporated into the scattering matrix S_N of the normal region, so we need not include it in r_A. It has the block form [27, 28]

$$\begin{aligned} r_\mathrm{A} &= \begin{pmatrix} \Gamma & \Lambda \\ \Lambda^* & \Gamma \end{pmatrix}, \quad \Gamma = \bigoplus_{m=1}^{M} \begin{pmatrix} \cos\alpha_m & 0 \\ 0 & \cos\alpha_m \end{pmatrix} \oplus \emptyset_Q \oplus \mathbb{1}_\zeta, \\ \Lambda &= \bigoplus_{m=1}^{M} \begin{pmatrix} 0 & -\mathrm{i}\sin\alpha_m \\ \mathrm{i}\sin\alpha_m & 0 \end{pmatrix} \oplus \mathbb{1}_Q \oplus \emptyset_\zeta. \end{aligned} \tag{1}$$

We have defined $\zeta = 0$ if the difference $N - Q$ is even and $\zeta = 1$ if $N - Q$ is odd, so that $N - Q - \zeta \equiv 2M$ is an even integer. The Andreev reflection eigenvalues $\rho_m = \sin^2\alpha_m$ that are not pinned at 0 or 1 are twofold degenerate [29][6].

The symbols $\mathbb{1}_n, \emptyset_n$ denote, respectively, an $n \times n$ unit matrix or null matrix for $n \geqslant 1$. The empty set is intended for $n = 0$. To make the notation more explicit, we give some examples of the direct sums,

$$\begin{aligned} &\mathbb{1}_1 \oplus \emptyset_1 = \begin{pmatrix} 1 & 0 \\ 0 & 0 \end{pmatrix}, \quad \mathbb{1}_2 \oplus \emptyset_1 = \begin{pmatrix} 1 & 0 & 0 \\ 0 & 1 & 0 \\ 0 & 0 & 0 \end{pmatrix}, \\ &\mathbb{1}_2 \oplus \emptyset_0 = \begin{pmatrix} 1 & 0 \\ 0 & 1 \end{pmatrix}, \quad \mathbb{1}_1 \oplus \emptyset_0 = 1, \quad \mathbb{1}_0 \oplus \emptyset_1 = 0. \end{aligned} \tag{2}$$

The normal region has a scattering matrix

$$S_\mathrm{N} = \begin{pmatrix} s_0 & 0 \\ 0 & s_0^* \end{pmatrix}, \quad s_0 = \begin{pmatrix} r' & t' \\ t & r \end{pmatrix}. \tag{3}$$

The electron and hole blocks (with $N \times N$ reflection and transmission matrices r, r', t, t') are each other's complex conjugate at the Fermi level. The off-diagonal blocks of S_N vanish, because the normal metal cannot mix electrons and holes. The matrix s_0 is unitary, $s_0 s_0^\dagger = 1$, without further restrictions in class D. In class BDI, chiral symmetry requires that $s_0 = s_0^\mathrm{T}$ is also a symmetric matrix.

To separate the mixing of modes from backscattering, we make use of the polar decomposition

$$s_0 = \begin{pmatrix} U & 0 \\ 0 & V \end{pmatrix} \begin{pmatrix} -\sqrt{1-\mathcal{T}} & \sqrt{\mathcal{T}} \\ \sqrt{\mathcal{T}} & \sqrt{1-\mathcal{T}} \end{pmatrix} \begin{pmatrix} U' & 0 \\ 0 & V' \end{pmatrix}. \tag{4}$$

[6] The Béri degeneracy of the Andreev reflection eigenvalues $\rho_m \neq 0, 1$ is a consequence of particle–hole symmetry, which is an anti-unitary symmetry that squares to +1. This distinguishes it from the more familiar Kramers degeneracy, resulting from an anti-unitary symmetry that squares to −1. For a self-contained proof of Béri degeneracy, see appendix B of [30].

The matrices U, V, U' and V' are $N \times N$ unitary matrices and $\mathcal{T} = \mathrm{diag}\,(T_1, T_2, \ldots, T_N)$ is a diagonal matrix of transmission eigenvalues of the normal region. In class BDI, chiral symmetry relates $U' = U^{\mathrm{T}}$, $V' = V^{\mathrm{T}}$.

2.2. Conductance

We combine S_{N} and r_{A} to obtain the matrix r_{he} of Andreev reflection amplitudes (from electron e to hole h) of the entire system. This calculation is much simplified in the case of $\zeta = 0$, $\rho_m = 1$ ($m = 1, 2, \ldots, M$) that all modes at the NS interface are Andreev reflected with unit probability. For this case $\Gamma = 0$, $N - Q = 2M$, we obtain

$$r_{he} = t'^{*}\Lambda^{*}(1 - r\Lambda r^{*}\Lambda^{*})^{-1}t, \quad \Lambda = \sigma_y^{\oplus M} \oplus \mathbb{1}_Q. \tag{5}$$

The notation $\sigma_y^{\oplus M}$ signifies the $2M \times 2M$ matrix constructed as the direct sum of M Pauli matrices.

The Andreev reflection matrix determines the conductance

$$G = G_0\,\mathrm{Tr}\,r_{he}r_{he}^{\dagger}, \quad G_0 = 2e^2/h. \tag{6}$$

Substitution of the polar decomposition (4) gives the compact expression

$$\begin{aligned} G/G_0 &= \mathrm{Tr}\,\mathcal{T}\mathcal{M}\mathcal{T}\mathcal{M}^{\dagger}, \\ \mathcal{M} &= (1 - \Omega^{*}\sqrt{1-\mathcal{T}}\Omega\sqrt{1-\mathcal{T}})^{-1}\Omega^{*}, \quad \Omega = V'\Lambda V^{*}. \end{aligned} \tag{7}$$

This is the zero-temperature conductance at the Fermi level, in the limit of zero bias voltage. Away from the Fermi level particle–hole symmetry is broken, so the electron and hole blocks in S_{N} are distinct unitary matrices s_{e} and s_{h}. If the bias voltage V_0 remains small compared to the excitation gap, we can keep the same r_{A}. The finite-voltage differential conductance $\tilde{G} = \mathrm{d}I/\mathrm{d}V_0$ is then given by

$$\begin{aligned} \tilde{G}/G_0 &= \mathrm{Tr}\,\mathcal{T}_{\mathrm{h}}\tilde{\mathcal{M}}\mathcal{T}_{\mathrm{e}}\tilde{\mathcal{M}}^{\dagger}, \\ \tilde{\mathcal{M}} &= (1 - \Omega_{\mathrm{h}}^{*}\sqrt{1-\mathcal{T}_{\mathrm{e}}}\Omega_{\mathrm{e}}\sqrt{1-\mathcal{T}_{\mathrm{h}}})^{-1}\Omega_{\mathrm{h}}^{*}, \\ \Omega_{\mathrm{e}} &= V_{\mathrm{e}}'\Lambda V_{\mathrm{h}}^{*}, \quad \Omega_{\mathrm{h}} = V_{\mathrm{h}}'\Lambda V_{\mathrm{e}}^{*}. \end{aligned} \tag{8}$$

The electron matrices are evaluated at energy eV_0 above the Fermi level and the hole matrices at energy $-eV_0$ below the Fermi level. Chiral symmetry remains operative away from the Fermi level; hence $V_{\mathrm{e}}' = V_{\mathrm{e}}^{\mathrm{T}}$, $V_{\mathrm{h}}' = V_{\mathrm{h}}^{\mathrm{T}} \Rightarrow \Omega_{\mathrm{h}} = \Omega_{\mathrm{e}}^{\dagger}$ in class BDI. We will apply equation (8) to voltages large compared to the Thouless energy, when the electron and hole matrices may be considered to be statistically independent.

2.3. Random matrix average

Isotropic mixing of the modes by scattering in the normal region means that the unitary matrices in the polar decomposition (4) are uniformly distributed in the unitary group $\mathcal{U}(N)$. We can calculate the average conductance for a given set of transmission eigenvalues by integration over $\mathcal{U}(N)$ with the uniform (Haar) measure. A full average would then still require an average over the T_n's, but if these are dominated by a tunnel barrier they will fluctuate a little and the partial average over the unitary matrices is already informative.

The calculation is easiest if all T_n's have the same value $0 \leqslant T \leqslant 1$. The average zero-voltage conductance $\langle G\rangle$ is then given by the integral

$$\langle G\rangle = T^2 G_0 \int_0^{2\pi} \mathrm{d}\phi\, \rho(\phi)\left|1-(1-T)\mathrm{e}^{\mathrm{i}\phi}\right|^{-2}, \tag{9}$$

with $\rho(\phi) = \langle \sum_n \delta(\phi-\phi_n)\rangle$ the density on the unit circle of the eigenvalues $\mathrm{e}^{\mathrm{i}\phi_n}$ of $\Omega\Omega^*$. The corresponding finite-voltage expression has a uniform $\rho = N/2\pi$, leading to

$$\langle \tilde{G}\rangle = NG_0T/(2-T), \tag{10}$$

irrespective of the symmetry class and independent of the topological quantum number Q.

The zero-voltage average (9) does depend on Q and is different for class D and BDI. The calculations are given in the appendix. Explicit expressions in class D are

$$\frac{\langle G\rangle_{\mathrm{D}}}{G_0} = \begin{cases} 2T, & \text{for } N=2,\ Q=0,\\ 1+2T^2, & \text{for } N=3,\ Q=1,\\ 2T(2-T+T^2), & \text{for } N=4,\ Q=0,\\ 1+2T^2(3-2T+T^2), & \text{for } N=5,\ Q=1. \end{cases} \tag{11}$$

The Q dependence appears to second order in the reflection probability $R = 1-T$, while the general first-order result

$$\langle G/G_0\rangle_{\mathrm{D}} = N(1-2R)+2R+\mathcal{O}(R^2) \tag{12}$$

is Q independent. The corresponding expressions in class BDI are more lengthy, and we only record the small-R result

$$\langle G/G_0\rangle_{\mathrm{BDI}} = N(1-2R)+2R\frac{Q^2+N}{N+1}+\mathcal{O}(R^2), \tag{13}$$

to show that it is Q-dependent already to first order in R. These are all finite-N results. In the large-N limit the Q dependence is lost,

$$\langle G/G_0\rangle = \frac{NT}{2-T}+\frac{2(1-T)}{(2-T)^2}+\mathcal{O}(N^{-1}), \tag{14}$$

irrespective of the symmetry class.

As illustrated in figure 2, for the case when all T_n's have the same value T the difference $\delta G = \langle G\rangle - \langle \tilde{G}\rangle$ is positive, corresponding to weak *anti*localization and a conductance *peak*. The sign of the effect may change if the T_n's are very different, in particular, in class BDI—which has $\delta G < 0$ in a quantum dot geometry (circular ensemble) [28]. It is a special feature of quantum interference in a magnetic field that the distinction between weak localization and antilocalization is not uniquely determined by the symmetry class [21, 31, 32].

3. Simulation of a microscopic model

The random-matrix calculation serves the purpose of a qualitative understanding of the weak antilocalization effect. For a quantitative description we need to relax the assumption of channel-independent T_n's. For that purpose we now turn to a microscopic model of a Majorana nanowire.

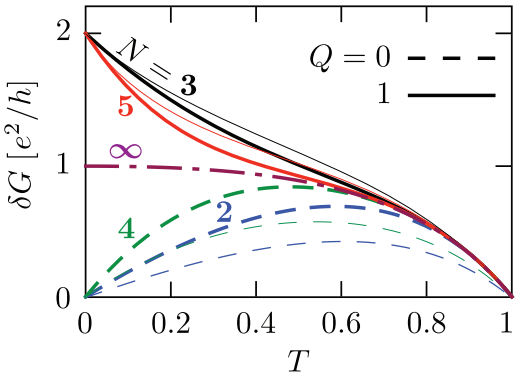

Figure 2. Amplitude δG of the average zero-voltage conductance peak as a function of (mode-independent) transmission probability T, in symmetry class D (thick curves) and BDI (thin curves) for different numbers of modes N. The superconductor is topologically trivial when N is even ($Q = 0$, dashed curves) and nontrivial when N is odd ($Q = 1$, solid curves). The dash-dotted curve is the Q-independent large-N limit (14).

3.1. Model Hamiltonian

Following [6, 7], we consider a conducting channel parallel to the x-axis on a substrate in the x–y-plane (width W and Fermi energy $E_{\rm F}$), in a magnetic field $\boldsymbol{B}$ (orientation $\hat{n}$ and Zeeman energy $E_{\rm Z} = \frac{1}{2} g_{\rm eff} \mu_{\rm B} B$), with Rashba spin–orbit coupling (characteristic energy $E_{\rm so} = m_{\rm eff}\alpha_{\rm so}^2/\hbar^2$ and length $l_{\rm so} = \hbar^2/m_{\rm eff}\alpha_{\rm so}$) and induced s-wave superconductivity (excitation gap Δ_0). The Hamiltonian is

$$\mathcal{H} = \begin{pmatrix} H_0 - E_{\rm F} & \Delta\sigma_y \\ \Delta^*\sigma_y & E_{\rm F} - H_0^* \end{pmatrix},$$
$$H_0 = \frac{p_x^2 + p_y^2}{2m_{\rm eff}} + U(x, y) + \frac{\alpha_{\rm so}}{\hbar}(\sigma_x p_y - \sigma_y p_x) + E_{\rm Z}\hat{n}\cdot\boldsymbol{\sigma}. \tag{15}$$

The electrostatic potential $U = U_{\rm gate} + \delta U$ contains the gate potential $U_{\rm gate}$ that creates the tunnel barrier and the impurity potential δU that varies randomly from site to site on a square lattice (lattice constant a), distributed uniformly in the interval $(-U_{\rm disorder}, U_{\rm disorder})$. The disordered region is $-L_{\rm N} < x < L_{\rm S}$, an NS interface is constructed by increasing the pair potential Δ from 0 to Δ_0 at $x = 0$ and a rectangular barrier of height $U_{\rm barrier}$, thickness $\delta L_{\rm barrier}$ is placed at $x = -x_{\rm barrier}$. The conductance of the normal region ($x < 0$) contains a contribution $G_{\rm disorder}$ from disorder and $G_{\rm barrier}$ from the barrier.

The orientation of the magnetic field plays an important role [6, 7]: it lies in the x–y-plane to eliminate orbital effects on the superconductor and we will only include its effect on the electron spin (through the Zeeman energy). A topologically nontrivial phase needs a nonzero excitation gap for $E_{\rm Z} > \Delta_0$, which requires a parallel magnetic field $B_\parallel$ ($\hat{n} = \hat{x}$). We will consider that case in the next subsection and then discuss the case of a perpendicular magnetic field $B_\perp$ ($\hat{n} = \hat{y}$) in section 3.3.

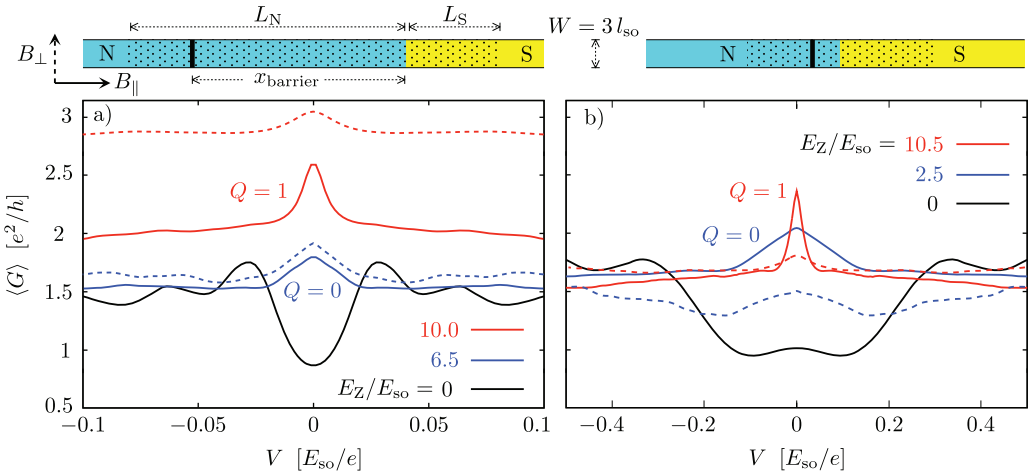

Figure 3. Disorder-averaged differential conductance as a function of bias voltage, for a nanowire modeled by Hamiltonian (15). The two panels (a) and (b) correspond to the two geometries shown to scale above each plot. (The solid vertical line indicates the position of the tunnel barrier, relative to the NS interface; disordered regions are dotted.) Each panel shows data for zero magnetic field (black) and for two nonzero magnetic field values (blue and red). The solid curves are for a parallel field $B_\parallel$ and the dashed curves for a perpendicular field $B_\perp$. The system is topologically trivial ($Q = 0$) in all the cases except for the red solid curves ($Q = 1$).[8]

3.2. Average versus sample-specific conductance

To avoid the complications from chiral symmetry, we first focus on a relatively wide junction, $W = 3\,l_{so}$, when symmetry class D (rather than BDI) applies [28]. (We turn to class BDI in the next subsection.) The normal region has $N = 8$ propagating modes (including spin) in zero magnetic field, for $E_F = 12\,E_{so}$. The topological quantum number Q was determined both from the determinant of the reflection matrix [33][7] and independently by counting the gap closings and reopenings upon increasing the magnetic field. A transition from $Q = 0$ to 1 is realized by increasing $B_\parallel$ at fixed $\Delta_0 = 8\,E_{so}$.

The results are shown in figure 3 (solid curves) for two geometries, one with the tunnel barrier far from the NS and another with the barrier close to the interface[8].

The disorder-averaged conductance shows a zero-voltage peak in a magnetic field, regardless of whether the nanowire is topologically trivial ($Q = 0$) or nontrivial ($Q = 1$). The peak disappears in zero magnetic field and instead a conductance minimum develops, indicative

[7] For the parallel magnetic fields in figures 3 and 4 we find that $Q = \frac{1}{2}(1 - \mathrm{Det}\,r)$ switches from 0 to 1 at $E_Z = 8.1\,E_{so}$ and then back to 0 at $E_Z = 11.3\,E_{so}$, with a re-entrant $Q = 0$ interval $9.2\,E_{so} < E_Z < 9.7\,E_{so}$

[8] The parameters for the simulations shown in figures 3 and 4 are, in panel (a): $x_{barrier} = 23\,l_{so}$, $\delta L_{barrier} = 4a = 0.4\,l_{so}$, $U_{disorder} = 12.5\,E_{so}$, $U_{barrier} = 15\,E_{so}$, $G_{disorder} = 2.7\,e^2/h$, $G_{barrier} = 1.8\,e^2/h$; in panel (b): $x_{barrier} = 3\,l_{so}$, $\delta L_{barrier} = a = 0.1\,l_{so}$, $U_{disorder} = 20\,E_{so}$, $U_{barrier} = 50\,E_{so}$, $G_{disorder} = 2.9\,e^2/h$ and $G_{barrier} = 3.2\,e^2/h$.

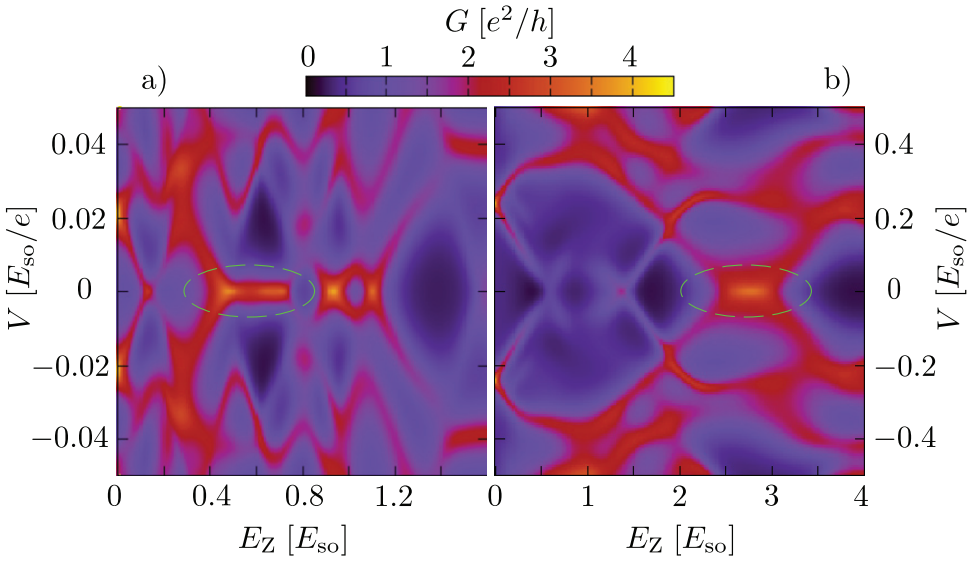

Figure 4. Numerical simulation of a nanowire for a single disorder realization (no averaging). The color scale gives the differential conductance as a function of bias voltage (the vertical axis) and parallel magnetic field (the horizontal axis). The parameters in panels (a) and (b) correspond to those in figures 3(a) and (b), as listed in footnote 8. The magnetic field range in both panels is in the topologically trivial phase ($Q = 0$), but still exhibits a conductance peak pinned to zero voltage (green circle).

of an induced superconducting minigap in the normal region. The two geometries in panels 3(a) and (b) show comparable results, the main difference being a broadening of the zero-bias peak when the tunnel barrier is brought closer to the NS interface—as expected from the increase in Thouless energy[9]. The shallow maximum which develops around zero voltage in the $B = 0$ curve of panel 3(b) is a precursor of the reflectionless tunneling peak, which appears in full strength when the barrier is placed at the NS interface [5].

All this applies to the average conductance in an ensemble of disordered nanowires. Individual members of the ensemble show mesoscopic, sample-specific conductance fluctuations, in addition to the systematic weak antilocalization effect. For some disorder realizations the zero-voltage conductance peak remains clearly visible, see figure 4. The peak sticks to zero bias voltage over a relatively wide magnetic field range, even though the superconductor is topologically trivial ($Q = 0$). The appearance and disappearance of the peak are not associated with the closing and reopening of an excitation gap, so it cannot produce Majorana fermions [34][10].

[9] Figure 3 shows that the $Q = 1$ peak becomes narrower than the $Q = 0$ peak when the length of the disordered region between the tunnel barrier and the NS interface is reduced. This is consistent with the findings of [17] for the effect of disorder on the Majorana resonance.

[10] The appearance and disappearance of the zero-voltage conductance peak in figure 4 are associated with the merging and splitting of two peaks at $\pm V_0$. We understand this as a collision of two poles of the scattering matrix at complex energy $i\varepsilon \pm V_0$, as described by Pikulin and Nazarov [34].

3.3. Parallel versus perpendicular magnetic field

So far we have considered a class D nanowire with a magnetic field $B_\parallel$ parallel to the wire axis. In a perpendicular magnetic field $B_\perp$ (perpendicular to the wire in the plane of the substrate) the symmetry class remains D (broken time-reversal and spin–rotation symmetry), although the topologically nontrivial phase disappears [6, 7]. We therefore expect the class D zero-bias peak to persist in a perpendicular field as a result of the weak antilocalization effect.

This expectation is borne out by the computer simulations, see the dashed curves in figure 3. A zero-bias peak exists for both $B_\perp$ and $B_\parallel$. If the nanowire is topologically trivial, there is not much difference in peak height for the two magnetic field directions (compare the blue solid and dashed curves). In contrast, if the nanowire is topologically nontrivial for a parallel field, then the peak is much reduced in a perpendicular field (red solid versus dashed curves). The disappearance of the Majorana zero mode and the collapse of the zero-bias peak may be accompanied by the appearance of propagating modes in the superconducting part of the nanowire. This explains the increased background conductance in the red dashed curve of figure 3(a).

The effect of a magnetic field rotation is entirely different when $W \lesssim l_{\rm so}$ and the symmetry class is BDI rather than D [26, 28]. The term $\sigma_x p_y$ in the Hamiltonian (15) can then be neglected, so that $\mathcal{H}$ commutes with σ_y in a perpendicular magnetic field ($\hat{n} = \hat{y}$). The two spin components along $\pm\hat{y}$ decouple and for each spin component separately the particle–hole symmetry is broken. We therefore expect both the Majorana resonance and the weak antilocalization peak to disappear in a perpendicular magnetic field for sufficiently narrow wires.

This is demonstrated by the computer simulations shown in figure 5, for the average conductance in a topologically trivial wire of width $W = 0.3\,l_{\rm so}$. The main difference with the data in figure 3 is that the symmetry class is now BDI rather than D, because of the narrower wire. This change of symmetry class does not significantly affect the weak antilocalization peak in a parallel magnetic field. But if the magnetic field is rotated to a perpendicular direction, the peak disappears—as expected for a class BDI nanowire.

3.4. Effects of thermal averaging

All the results presented so far are in the zero-temperature limit. We calculate the temperature dependence of the differential conductance from the finite-T_0 and finite-V_0 generalization of equation (6),

$$G = \frac{2e}{h}\int_{-\infty}^{\infty} {\rm d}\varepsilon\, \frac{{\rm d}f(\varepsilon - eV_0)}{{\rm d}V_0}\, {\rm Tr}\, r_{he}(\varepsilon) r_{he}^\dagger(\varepsilon), \tag{16}$$

$$f(\varepsilon) = \frac{1}{1+\exp(\varepsilon/k_{\rm B}T_0)}. \tag{17}$$

Thermal averaging at a nonzero temperature T_0 broadens the conductance peak around $V_0 = 0$ and reduces its height, at constant area $\int G\,{\rm d}V_0$ under the peak.

This effect of thermal averaging applies to both the weak antilocalization peak and the Majorana resonance, but the characteristic temperature scale is different, as shown in figure 6.

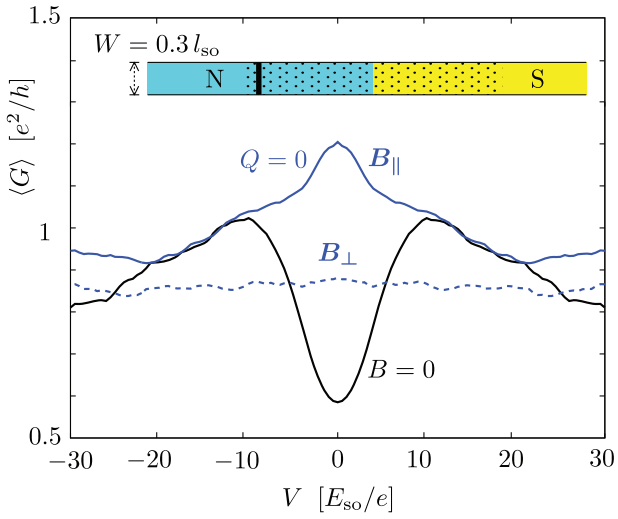

Figure 5. The same as figure 3, but now for a narrower wire in symmetry class BDI (rather than D). The system is topologically trivial, without Majorana zero modes. The weak antilocalization peak vanishes if the magnetic field is rotated from $B_\parallel$ to $B_\perp$.[11]

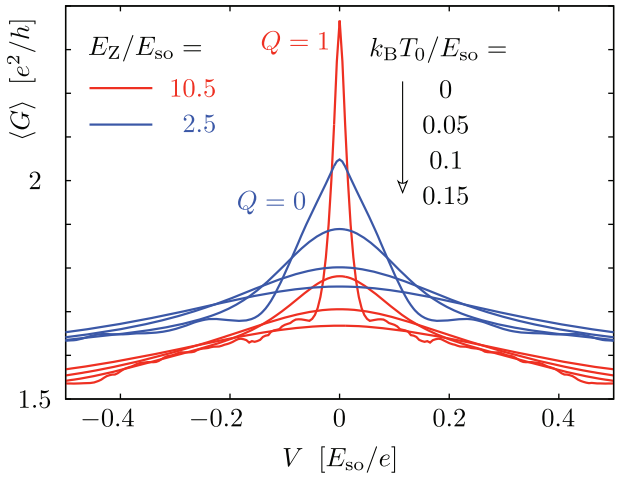

Figure 6. Temperature dependence of the conductance peaks from figure 3(b). The four blue curves ($Q = 0$, topologically trivial) correspond from top to bottom to four increasing temperatures and likewise the four red curves ($Q = 1$, topologically nontrivial).

The Majorana zero mode is more sensitive to thermal averaging because it is more tightly bound to the NS interface, with a smaller Thouless energy and therefore a smaller characteristic temperature.

[11] The parameters for the simulations shown in figure 5 are: $W = 0.3\,l_{\rm so}$, $x_{\rm barrier} = 2.7\,l_{\rm so}$, $\delta L_{\rm barrier} = a = 0.01\,l_{\rm so}$, $E_{\rm F} = 1000\,E_{\rm so}$, $\Delta_0 = 100\,E_{\rm so}$, $U_{\rm disorder} = 4000\,E_{\rm so}$ and $U_{\rm barrier} = 7000\,E_{\rm so}$, corresponding to $N = 8$, $G_{\rm disorder} = 1.3\,e^2/h$ and $G_{\rm barrier} = 1.5\,e^2/h$.

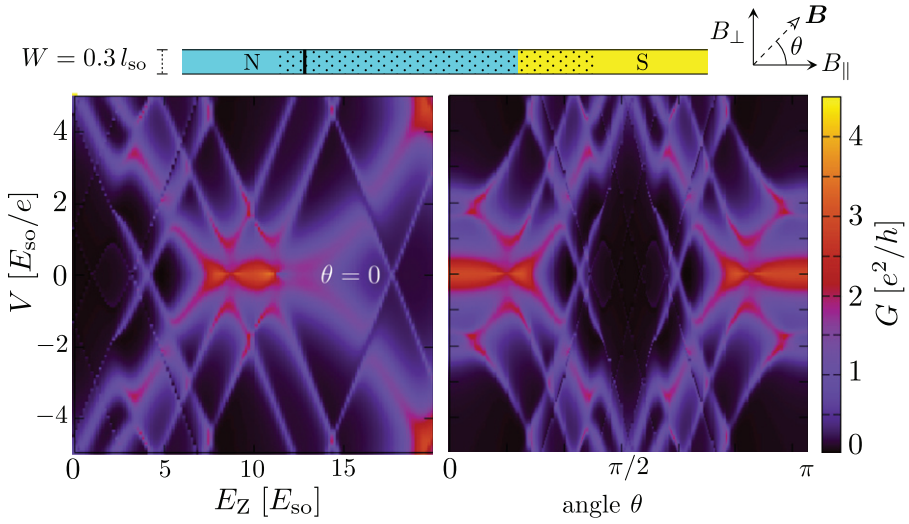

Figure 7. Differential conductance for a single disorder realization of a nanowire ($N = 2$ spin-resolved modes)[12]. The left panel shows the appearance of a zero-voltage peak in a range of magnetic field values, for $\boldsymbol{B}$ parallel to the wire. The right panel shows the dependence on the orientation of the magnetic field, for a fixed field strength ($E_{\rm Z} = 10\,E_{\rm so}$). The zero-voltage peak vanishes if $\boldsymbol{B}$ is perpendicular to the wire. This is the same phenomenology as for a Majorana resonance, but here it happens in the topologically trivial phase.

4. Discussion

In conclusion, we have shown that random quantum interference by disorder in a superconducting nanowire can systematically produce a zero-voltage conductance peak in the absence of time-reversal symmetry. This weak antilocalization effect relies on the same particle–hole symmetry that protects the Majorana zero mode, but it exists in both the topologically trivial and nontrivial phases of the superconductor. A conclusive demonstration of Majorana fermions will need to rule out this alternative mechanism for a conductance peak.

There are several strategies one might follow for this purpose:

- Increasing the tunnel barrier with a gate voltage suppresses the weak antilocalization effect, but not the Majorana resonance. The resonance does become narrower, so at finite temperatures thermal smearing will still lead to a suppression with increasing barrier height and this might not be the most effective strategy to distinguish the two effects.
- The disappearance of the conductance peak when the magnetic field is rotated (in the plane of the substrate) towards a direction perpendicular to the wire, the technique used in [10, 12], can identify the Majorana zero mode—but only if the ratio $W/l_{\rm so}$ is sufficiently large that the wire is in class D rather than BDI. In class BDI the Zeeman energy in the rotated field commutes with the Rashba energy, precluding the weak antilocalization effect

[12] The parameters for the simulations shown in figure 7 are: $W = 0.3\,l_{\rm so}$, $x_{\rm barrier} = 1.1\,l_{\rm so}$, $\delta L_{\rm barrier} = a = 0.01\,l_{\rm so}$, $E_{\rm F} = 200\,E_{\rm so}$, $\Delta_0 = 100\,E_{\rm so}$, $E_{\rm Z} = 60\,E_{\rm so}$, $U_{\rm disorder} = 500\,E_{\rm so}$ and $U_{\rm barrier} = 2000\,E_{\rm so}$, corresponding to $N = 2$, $G_{\rm disorder} = 1.5\,e^2/h$ and $G_{\rm barrier} = 0.85\,e^2/h$.

as well as the Majorana resonance. Both the works [10, 12] have $W \lesssim l_{\rm so}$ and are believed to be in class BDI [16, 26], so this complication seems quite relevant.

- Measuring the conductance through a single-mode point contact is a very effective strategy: for $N = 1$ the zero-temperature conductance $G = Q \times 2e^2/h$ directly measures the topological quantum number even without any tunnel barrier [35], and this signature of a Majorana zero mode is quite robust against finite temperatures. (The chararacteristic energy scale is the induced superconducting gap in the region between the point contact and the superconductor.) The single mode in the point contact should be spin resolved for this to work: if instead the point contact transmits both spins in one orbital mode ($N = 2$), then the ambiguity between weak antilocalization and the Majorana resonance remains (see figure 7).
- The Majorana resonance from a wire of finite length should split into two at the lowest temperatures, because of the nonzero overlap of the zero modes at the two ends of the wire [12]. No such systematic splitting will occur for the weak antilocalization peak.

Acknowledgments

We have benefited from discussions with A R Akhmerov and Yu V Nazarov. Numerical simulations of the nanowire were performed with the kwant software package, developed by A R Akhmerov, C W Groth, X Waintal and M Wimmer. This research was supported by the Dutch Science Foundation (NWO/FOM) and by an ERC Advanced Investigator grant.

Appendix. Random-matrix theory

To evaluate the average conductance (9) we seek the density of the eigenvalues $x_n = {\rm e}^{{\rm i}\phi_n}$ of the product $X = \Omega\Omega^*$ of the unitary matrix Ω and its complex conjugate. We denote $\mu_n = \cos\phi_n \in [-1, 1]$ and determine the joint probability distribution $P(\{\mu_n\})$ using methods from random-matrix theory [36].

In symmetry class D, we have $\Omega = V'\Lambda V^*$ with V and V' independently and uniformly distributed according to the Haar measure ${\rm d}U$ of the unitary group $\mathcal{U}(N)$. Because ${\rm d}(UU')={\rm d}U$ for a fixed unitary matrix U', the matrix $\Omega \equiv U$ is itself uniformly distributed in $\mathcal{U}(N)$.

In class BDI, we have $V' = V^{\rm T}$ and we may write $\Omega \equiv U\lambda U^\dagger$ with U uniformly in $\mathcal{U}(N)$. The diagonal matrix $\lambda = {\rm diag}(\lambda_1, \lambda_2, \ldots, \lambda_N)$ contains the eigenvalues $\lambda_n = \pm 1$ of Λ. The number $q = |Q|$ of Majorana zero modes is encoded in the topological invariant $Q = {\rm Tr}\,\Lambda = \sum_n \lambda_n$. (For full generality we allow Q to also take on negative values, but the final result will only depend on the absolute value q.)

A.1. Brownian motion of unitary matrices

We employ Dyson's Brownian motion approach [37], which sets up a stochastic process for the unitary matrix U whose stationary distribution coincides with the Haar measure on $\mathcal{U}(N)$. In each infinitesimal step of the process, $U \to U\exp({\rm i}H)$, where H is a Hermitian matrix from the Gaussian unitary ensemble, with identically normal distributed complex numbers $H_{lm} = H^*_{ml}$ ($l \leqslant m$), $\overline{H_{lm}} = 0$, $\overline{H_{kl}H_{mn}} = \delta_{kn}\delta_{lm}\tau$, $\overline{H_{kl}H^*_{mn}} = \delta_{km}\delta_{ln}\tau$; the limit $\tau \to 0$ is implied to generate infinitesimal increments.

The corresponding increments $\delta\mu_n$ can be calculated in perturbation theory. The drift coefficients $c_l = \lim_{\tau\to 0} \tau^{-1}\overline{\delta\mu_l}$ and the diffusion coefficients $c_{lm} = \lim_{\tau\to 0} \tau^{-1}\overline{\delta\mu_l\delta\mu_m}$ follow by averaging over the random variables in H. As we will see, the symmetries in the classes D and BDI are restrictive enough so that these coefficients can be expressed in terms of the quantities μ_n alone, without requiring data from the eigenvectors of X. Thus, the stochastic process for these quantities closes.

Introducing a fictitious time t, the evolution of the joint probability distribution is governed by a Fokker–Planck equation,

$$\frac{\partial P}{\partial t} = \left[-\sum_l \frac{\partial}{\partial \mu_l} c_l + \frac{1}{2} \sum_{l,m} \frac{\partial}{\partial \mu_l} \frac{\partial}{\partial \mu_m} c_{lm} \right] P\left(\{\mu_n\}, t\right). \tag{A.1}$$

The stationary solution $P(\{\mu_n\})$, for which the right-hand side of the Fokker–Planck equation vanishes, is the required eigenvalue distribution.

A.2. Symmetry class D

In class D, we have $X = UU^*$ with U uniformly distributed in $\mathcal{U}(N)$. Note that the operation of complex conjugation is basis dependent; if $B = A^*$ in one basis, then this relation is only preserved under orthogonal transformations, but not under general unitary transformations. Thus, we work in a fixed basis $|r\rangle$ (at most permitting orthogonal basis changes), and define for any $|\psi\rangle = \sum_r \psi_r |r\rangle$ a complex-conjugated vector $|\psi^*\rangle \equiv \sum_r \psi_r^* |r\rangle$. As usual, $\langle\psi| = \sum_r \psi_r^* \langle r|$; thus $\langle\psi^*| = \sum_r \psi_r \langle r|$.

The matrices X and U are unitary and obey $\mathrm{Det}\, X = |\mathrm{Det}\, U|^2 = 1$. Moreover, the matrix X^* has the same eigenvalues $x_1, x_2, \ldots, x_N$ as the matrix X. For even N, it follows that all eigenvalues appear in complex-conjugated pairs; every eigenvalue x_k has a partner $x_{\bar{k}} = x_k^* = x_k^{-1}$. For odd N, in addition to such pairs there is a single unpaired eigenvalue, denoted as x_N, which (because of the constraint on the determinant) is pinned at $x_N = 1$. The paired eigenvectors are related according to

$$|\bar{k}\rangle = \xi_k U |k^*\rangle. \tag{A.2}$$

Here we have to set ξ_k such that $\xi_k^2 = \lambda_k$; this guarantees that the relation between both eigenvectors in a pair is reciprocal, $|\bar{\bar{k}}\rangle = |k\rangle$. Observing that the eigenvectors form an orthogonal basis, we find the matrix elements

$$\langle k|U|l^*\rangle = \xi_k \delta_{k\bar{l}} = (\langle k^*|U^*|l\rangle)^* = \langle l|U^{\mathrm{T}}|k^*\rangle. \tag{A.3}$$

With the help of these matrix elements we can now evaluate the drift and diffusion coefficients. In second-order perturbation theory,

$$\delta x_l = \langle l|\delta X|l\rangle + {\sum_k}' \frac{\langle l|\delta X|k\rangle\langle k|\delta X|l\rangle}{x_l - x_k}, \tag{A.4}$$

where the prime restricts the sum to $k \neq l$, while

$$\delta X = \mathrm{i}U H U^* - \mathrm{i}X H^* + U H U^* H^* - \frac{1}{2} U H^2 U^* - \frac{1}{2} X H^{*2} \tag{A.5}$$

is the increment of X to leading order in τ. The Gaussian averages are now carried out according to the rules

$$\langle k|AHB|l\rangle\langle m|CHD|n\rangle = \tau\langle k|AD|n\rangle\langle m|CB|l\rangle, \tag{A.6}$$

$$\langle k|AHB|l\rangle\langle m|CH^*D|n\rangle = \tau\langle k|AC^{\mathrm{T}}|m^*\rangle\langle n^*|D^{\mathrm{T}}B|l\rangle. \tag{A.7}$$

In particular, $\overline{H^2} = N\tau$, $\overline{UHU^*H^*} = \tau UU^\dagger = \tau$, and

$$\begin{aligned}\overline{\langle l|UHU^* - XH^*|k\rangle\langle k|UHU^* - XH^*|l\rangle}&\\ = 2\tau\langle l|X|l\rangle\langle k|X|k\rangle - \tau\langle l|U^{\mathrm{T}}|k^*\rangle\langle l^*|U^*|k\rangle - \tau\langle k|U^{\mathrm{T}}|l^*\rangle\langle k^*|U^*|l\rangle&\\ = 2\tau x_l x_k - \tau\delta_{l\bar{k}}(x_l + x_{\bar{l}}),&\end{aligned} \tag{A.8}$$

where we invoked equation (A.3). We thus obtain

$$\overline{\delta x_l} = \tau - N\tau x_l - \tau{\sum_k}' \frac{2x_l x_k - \delta_{l\bar{k}}(x_l + x_{\bar{l}})}{x_l - x_k}. \tag{A.9}$$

Analogously, we find that

$$\overline{\delta x_l \delta x_m} = \overline{\langle l|\delta X|l\rangle\langle m|\delta X|m\rangle} = -2\tau\delta_{lm}x_l^2 + 2\tau\delta_{l\bar{m}}. \tag{A.10}$$

Note that these expressions only depend on the eigenvalues. We remark that for the pinned unpaired eigenvalue $x_N = 1$, occurring if N is odd, these relations deliver $\overline{\delta x_N} = \overline{(\delta x_N)^2} = 0$.

We now pass over to the quantities $\mu_l = (x_l + x_{\bar{l}})/2$, and restrict the index l such that it enumerates the pairs of eigenvalues. For even N we then find that

$$\overline{\delta\mu_l} = \tau - 2\tau\mu_l - 2\tau(\mu_l^2 - 1){\sum_k}' \frac{1}{\mu_l - \mu_k}, \tag{A.11}$$

while for odd N we have

$$\overline{\delta\mu_l} = -3\tau\mu_l - 2\tau(\mu_l^2 - 1){\sum_k}'' \frac{1}{\mu_l - \mu_k}, \tag{A.12}$$

where the double prime excludes the pinned eigenvalue. Furthermore,

$$\overline{\delta\mu_l\delta\mu_m} = 2\tau(1 - \mu_l^2)\delta_{lm}. \tag{A.13}$$

The stationarity condition of the associated Fokker–Planck equation (A.1) can be expressed as

$$\frac{\partial}{\partial\mu_l}\overline{\delta\mu_l}P = \frac{1}{2}\frac{\partial^2}{\partial\mu_l}\overline{(\delta\mu_l)^2}P. \tag{A.14}$$

For even $N = 2M$, this is solved by

$$P(\mu_1, \mu_2, \ldots, \mu_M) \propto \prod_{k=1}^{M} \frac{1+\mu_k}{\sqrt{1-\mu_k^2}} \prod_{l<m=1}^{M} (\mu_l - \mu_m)^2, \tag{A.15a}$$

up to a normalization constant. Each of the μ_n's ($n = 1, 2, \ldots, M$) is twofold degenerate. For odd $N = 2M + 1$ one eigenvalue is pinned at +1, and the remaining ones are twofold degenerate with the distribution

$$P(\mu_1, \mu_2, \ldots, \mu_M) \propto \prod_{k=1}^{M} \sqrt{1-\mu_k^2} \prod_{l<m=1}^{M} (\mu_l - \mu_m)^2. \tag{A.15b}$$

This concludes our derivation of the eigenvalue distribution of UU^* with U uniform in $\mathcal{U}(N)$. We have not found the result (A.15) in the literature, but there is a curious correspondence with the known [36, 38] eigenvalue distribution of orthogonal matrices (uniformly distributed according to the Haar measure). An $(N+1)\times(N+1)$ orthogonal matrix O with determinant -1 has one eigenvalue pinned at -1. If we exclude that eigenvalue, the remaining N eigenvalues of O have the same probability distribution as the N eigenvalues of UU^*.

A.3. Brownian motion of orthogonal matrices

As an independent demonstration of this correspondence between the eigenvalue distributions of UU^* and O, we have investigated the Brownian motion of orthogonal matrices. Let O be a random $(N+1)\times(N+1)$-dimensional matrix in the orthogonal group, constrained to the sector $\mathrm{Det}\, O=-1$.

The Brownian motion is induced by $O(1+A+A^2/2)$, where (in the fixed basis) $A=-A^{\mathrm{T}}$ is a real antisymmetric matrix, with $\overline{A_{lm}^2}=\tau$. Due to the condition on the determinant, there is always one eigenvalue pinned at $x_{N+1}=-1$, while an additional eigenvalue is pinned at $x_N=1$ if N is odd. All other eigenvalues appear in pairs x_l, $x_{\bar{l}}$, with $|\bar{l}\rangle=|l^*\rangle$ (no additional factors are required).

We calculate the increments and average:

$$\begin{aligned}\delta x_l &= \frac{1}{2}\langle l|OA^2|l\rangle+\sum_{k\neq l}\frac{\langle l|OA|k\rangle\langle k|OA|l\rangle}{x_l-x_k}\\ &\Rightarrow \overline{\delta x_l}=-\frac{1}{2}\tau N x_l+\tau\sum_{k\neq l}\frac{x_l x_k(\delta_{k\bar{l}}-1)}{x_l-x_k},\end{aligned}\tag{A.16}$$

$$\begin{aligned}\delta x_l\delta x_k &= \langle l|OA|l\rangle\langle k|OA|k\rangle\\ &\Rightarrow \overline{\delta x_l\delta x_k}=\tau x_l x_k(\delta_{l\bar{k}}-\delta_{lk})=\tau(\delta_{l\bar{k}}-x_l^2\delta_{lk}).\end{aligned}\tag{A.17}$$

(Note that $\langle l|A|l\rangle$ does not vanish if $|l\rangle$ is complex, as is generally the case for the unpinned eigenvalues.)

As before, in passing to μ_l we restrict indices to enumerate different pairs. For N even, we find that (considering that the restricted sum has $(N-2)/2$ terms)

$$\begin{aligned}\overline{\delta\mu_l} &= \frac{1}{2}\tau-\frac{1}{2}\tau N\mu_l-\tau\sum_{k\neq l,N+1}\frac{\mu_l\mu_k-1}{\mu_l-\mu_k}\\ &= \frac{1}{2}\tau-\tau\mu_l-\tau(\mu_l^2-1)\sum_{k\neq l,N+1}\frac{1}{\mu_l-\mu_k},\end{aligned}\tag{A.18}$$

while if N is odd (where the restricted sum has $(N-3)/2$ terms),

$$\begin{aligned}\overline{\delta\mu_l} &= -\frac{1}{2}\tau N\mu_l-\tau\sum_{k\neq l,N,N+1}\frac{\mu_l\mu_k-1}{\mu_l-\mu_k}\\ &= -\frac{3}{2}\tau\mu_l-\tau(\mu_l^2-1)\sum_{k\neq l,N,N+1}\frac{1}{\mu_l-\mu_k}.\end{aligned}\tag{A.19}$$

Furthermore,

$$\overline{\delta\mu_l\delta\mu_k} = \tau(1-\mu_l^2)\delta_{lk}. \tag{A.20}$$

Comparison with equations (A.11)–(A.13) shows that these are the same average increments, if we rescale τ by a factor of 2. The eigenvalues of UU^* and O therefore execute the same Brownian motion process, with the same stationary solution (A.15).

A.4. Symmetry class BDI

In class BDI, we have $X = U\lambda U^\dagger U^*\lambda U^{\mathrm{T}}$, with U uniform in $\mathcal{U}(N)$ and λ a fixed diagonal matrix with entries ±1 that sum up to Q. Since here the matrix X is symmetric, $X = X^{\mathrm{T}}$, it is now diagonalized by an orthogonal transformation; thus, the eigenvectors $|k\rangle = |k^*\rangle$ are real. As in class D, eigenvalues appear in complex-conjugate pairs, apart from eigenvalues pinned at 1. We observe that Ω mediates between the associated eigenvector, $|\bar{k}\rangle = \xi_k\Omega|k\rangle = \xi_k^*\Omega^*|k\rangle$. In order to treat the partners symmetrically we have to require that $|\bar{k}\rangle$ is also real, so ξ_k compensates for any complex overall factor. It then follows that $\langle k|\Omega\Omega^*|k\rangle = \xi_k^2 = \lambda_k$, and thus the coefficients ξ_k are related to the eigenvalues as in class D.

To identify the pinned eigenvalues note that $\Omega = \Omega^\dagger = \Omega^{-1}$ is both Hermitian and unitary, and thus has eigenvalues ±1. Let $\Omega_\pm$ be the eigenspace for each set of eigenvalues, and $\Omega_\pm^*$ the analogous eigenspace for Ω^*, which is spanned by the complex-conjugated vectors. We denote $\xi = \operatorname{sign} Q$. The space $[\operatorname{span}(\Omega_{-\xi}, \Omega_{-\xi}^*)]^\perp$ is then of dimension $q = |Q|$ (barring accidental degeneracies), and all of the vectors in this space obey $X|k\rangle = |k\rangle$. Thus X has $q = |Q|$ eigenvalues pinned at 1. For each pinned eigenvalue, insisting that $|\bar{k}\rangle = |k\rangle$ implies $\Omega|k\rangle = \Omega^*|k\rangle = \xi|k\rangle$, $\xi = \operatorname{sign} Q = \pm1$ (consistent with the property that these states lie in the joint subspace of Ω_ξ and Ω_ξ^*).

With these additional properties in hand, the evaluation of drift and diffusion coefficients can proceed along the same steps as before. With the specified form of X, the incremental step of U carries over to an increment

$$\begin{aligned}\delta X = {}& \mathrm{i}U[H,\lambda]U^\dagger\Omega^* - \mathrm{i}\Omega U^*[H^*,\lambda]U^{\mathrm{T}} \\ & + \tau Q(\Omega^*+\Omega) + 2\tau(1-X) - 2N\tau X,\end{aligned} \tag{A.21}$$

where we have already averaged terms of second order in H; in particular, terms such as $\overline{UH\lambda HU^\dagger U^*\lambda U^{\mathrm{T}}} = \tau Q\Omega^*$ produce the topological invariant Q. The associated eigenvalue increment averages to

$$\begin{aligned}\overline{\delta x_l} &= -2N\tau x_l + \tau Q\langle l|\Omega^*+\Omega|l\rangle + 2\tau(1-x_l) \\ &\quad -{\sum_k}' (x_l-x_k)^{-1}\overline{\langle l|U[H,\lambda]U^\dagger\Omega^* - \Omega U^*[H^*,\lambda]U^{\mathrm{T}}|k\rangle\langle k|U[H,\lambda]U^\dagger\Omega^* - \Omega U^*[H^*,\lambda]U^{\mathrm{T}}|l\rangle} \\ &= -2N\tau x_l + 2\tau q\delta_{l\bar{l}} + 2\tau(1-x_l) - 4\tau{\sum_k}' \frac{x_lx_k - \delta_{l\bar{l}}\delta_{k\bar{k}} - \delta_{k\bar{l}}(x_l+x_{\bar{l}})/2 + x_lx_k\delta_{lk}}{x_l-x_k},\end{aligned} \tag{A.22}$$

where the δ_{lk} term can be dropped because of the constraint $k \neq l$ on the sum. Note how Q changes to $q = |Q|$ because of the sign of the matrix element involving pinned eigenvalues.

Again we find that eigenvalues at unity remain pinned. For the other eigenvalues, we separate out from the sum the q eigenvalues that are pinned, and sum over the $M = (N-q)/2$

pairs of unpinned eigenvalues,

$$\begin{aligned}\overline{\delta x_l} = &-2N\tau x_l + 2\tau(1-x_l) - 2\tau\frac{2-(x_l+x_{\bar{l}})}{x_l - x_{\bar{l}}} \\ &- 4\tau q\frac{x_l}{x_l-1} - 4\tau x_l{\sum_k}'' \frac{x_k + x_{\bar{k}} - 2x_{\bar{l}}}{x_l + x_{\bar{l}} - x_k - x_{\bar{k}}},\end{aligned} \tag{A.23}$$

where the double prime again indicates the exclusion of the pinned eigenvalues. Furthermore,

$$\overline{\delta x_l \delta x_m} = 8\tau(\delta_{l\bar{m}} - \delta_{lm}x_l^2). \tag{A.24}$$

For the quantities $\mu_l = (x_l + x_{\bar{l}})/2$, this gives

$$\overline{\delta\mu_l} = -2q\tau(\mu_l+1) + 2\tau(1-3\mu_l) - 4\tau{\sum_k}''\frac{\mu_l^2-1}{\mu_l-\mu_k}, \tag{A.25}$$

$$\overline{\delta\mu_l\delta\mu_m} = 8\tau(1-\mu_l^2)\delta_{lm}. \tag{A.26}$$

The stationarity condition (A.14) is now fulfilled for

$$P(\mu_1, \mu_2, \ldots, \mu_M) \propto \prod_{k=1}^{M}(1-\mu_k)^{(q-1)/2} \prod_{l<m=1}^{M} |\mu_l - \mu_m|, \tag{A.27}$$

which gives the joint probability distribution of the twofold degenerate, unpinned eigenvalues μ_n $(n = 1, 2, \ldots, M)$.

A.5. Eigenvalue density

The probability distributions (A.15) and (A.27) are both of the form

$$P(\mu_1, \mu_2, \ldots, \mu_M) \propto \prod_{k=1}^{M}(1+\mu_k)^a(1-\mu_k)^b \prod_{l<m=1}^{M} |\mu_l - \mu_m|^\beta, \tag{A.28}$$

with $\beta = 2$, $a = 1/2$, $b = |Q| - 1/2$ in class D and $\beta = 1$, $a = 0$, $b = |Q|/2 - 1/2$ in class BDI. These are called Jacobi distributions, because the eigenvalue density $\rho(\mu)$ can be written in terms of Jacobi polynomials [36].

For small N it is easier to calculate the eigenvalue density by integrating out all μ_n's except a single one. Keep in mind that $|Q|$ of the μ_n's are pinned at unity and that the $N - |Q| = 2M$ unpinned μ_n's are twofold degenerate. (The products in equation (A.28) run only over these M unpinned pairs.) The eigenvalue density $\rho(\mu) = \langle\sum_{n=1}^{N}\delta(\mu-\mu_n)\rangle$ is then given by

$$\begin{aligned}\rho(\mu) &= |Q|\delta(\mu-1) + 2Mp(\mu), \\ p(\mu) &= \int_{-1}^{1}\mathrm{d}\mu_1\int_{-1}^{1}\mathrm{d}\mu_2 \\ &\quad\cdots\int_{-1}^{1}\mathrm{d}\mu_M\,\delta(\mu-\mu_1)P(\mu_1,\mu_2,\ldots,\mu_M).\end{aligned} \tag{A.29}$$

The delta functions satisfy $\int_{-1}^{1}\delta(\mu\pm1)\mathrm{d}\mu=1$. The average conductance follows from the eigenvalue density according to equation (9),

$$\langle G\rangle = T^2G_0\int_{-1}^{1}\mathrm{d}\mu\,\rho(\mu)[1+(1-T)^2-2(1-T)\mu]^{-1}. \tag{A.30}$$

This gives the small-N results in equation (11) and figure 2.

The large-N limit (14) is obtained from an integral equation for the eigenvalue density in the Jacobi ensemble [5, 39],

$$M\int_{-1}^{1}\mathrm{d}\mu\,p(\mu')\ln|\mu-\mu'| = -\frac{1}{2}(1-2/\beta)\ln p(\mu) - \frac{a}{\beta}\ln(1+\mu)-\frac{b}{\beta}\ln(1-\mu)+C+\mathcal{O}(1/M). \tag{A.31}$$

The constant C is determined by the normalization

$$\int_{-1}^{1}\mathrm{d}\mu\,p(\mu)=1. \tag{A.32}$$

The solution is

$$Mp(\mu) = \frac{\tilde{M}}{\pi\sqrt{1-\mu^2}}-\frac{a}{\beta}\delta(\mu+1)-\frac{b}{\beta}\delta(\mu-1) + \frac{1}{4}(1-2/\beta)[\delta(\mu+1)+\delta(\mu-1)]+\mathcal{O}(1/M), \tag{A.33}$$

$$\tilde{M} = M+(a+b)/\beta-\frac{1}{2}(1-2/\beta). \tag{A.34}$$

Upon substitution of the values for a, b, β into the two symmetry classes and transforming back from p to ρ, we find that

$$\rho(\mu) = \frac{N}{\pi}\frac{1}{\sqrt{1-\mu^2}}+\frac{1}{2}\delta(\mu-1)-\frac{1}{2}\delta(\mu+1)+\mathcal{O}(1/M), \tag{A.35}$$

independent of Q and for both symmetry classes D and BDI. The corresponding result for the conductance is equation (14), to order $1/N$ if the limit $N\to\infty$ is taken at a fixed Q.

A.6. Large-voltage limit

For completeness we also give the derivation of the large-voltage limit (10) of the average conductance. We need to evaluate

$$\langle\tilde{G}\rangle = T^2G_0\int_0^{2\pi}\mathrm{d}\phi\,\tilde{\rho}(\phi)\left|1-(1-T)\mathrm{e}^{\mathrm{i}\phi}\right|^{-2}, \tag{A.36}$$

with $\tilde{\rho}(\phi)=\langle\sum_n\delta(\phi-\phi_n)\rangle$ the density on the unit circle of the eigenvalues $\mathrm{e}^{\mathrm{i}\phi_n}$ of a unitary matrix $\tilde{\Omega}$.

In class D, the matrix $\tilde{\Omega}\equiv U$ is uniformly distributed in $\mathcal{U}(N)$. This is the circular unitary ensemble (CUE, $\beta=2$). In class BDI, the chiral symmetry enforces that $\tilde{\Omega}$ is unitary symmetric, $\tilde{\Omega}=UU^{\mathrm{T}}$ with U uniform in $\mathcal{U}(N)$. This is the circular orthogonal ensemble (COE, $\beta=1$).

Unlike the probability distributions we needed for the zero-voltage limit, these two distributions are in the literature [36],

$$P(\phi_1, \phi_2, \ldots, \phi_N) \propto \prod_{k<l=1}^{N} |e^{i\phi_k} - e^{i\phi_l}|^{\beta}. \tag{A.37}$$

The corresponding density

$$\tilde{\rho}(\phi) = N/2\pi, \quad 0 < \phi \leqslant 2\pi \tag{A.38}$$

is uniform irrespective of the value of β and without any finite-N corrections. Substitution into equation (A.37) gives the result (10).

References

[1] Bergmann G 1984 *Phys. Rep.* **107** 1
[2] Lee P A and Ramakrishnan T V 1985 *Rev. Mod. Phys.* **57** 287
[3] Brouwer P W and Beenakker C W J 1995 *Phys. Rev.* B **52** 3868
[4] Altland A and Zirnbauer M R 1996 *Phys. Rev. Lett.* **76** 3420
[5] Beenakker C W J 1997 *Rev. Mod. Phys.* **69** 731
[6] Lutchyn R M, Sau J D and Das Sarma S 2010 *Phys. Rev. Lett.* **105** 077001
[7] Oreg Y, Refael G and von Oppen F 2010 *Phys. Rev. Lett.* **105** 177002
[8] Alicea J 2012 *Rep. Prog. Phys.* **75** 076501
Beenakker C W J 2011 arXiv:1112.1950
[9] Law K T, Lee P A and Ng T K 2009 *Phys. Rev. Lett.* **103** 237001
[10] Mourik V, Zuo K, Frolov S M, Plissard S R, Bakkers E P A M and Kouwenhoven L P 2012 *Science* **336** 1003
[11] Deng M T, Yu C L, Huang G Y, Larsson M, Caroff P and Xu H Q 2012 arXiv:1204.4130
[12] Das A, Ronen Y, Most Y, Oreg Y, Heiblum M and Shtrikman H 2012 *Nature Phys.* **8** 887–95
[13] Wilson R M 2012 *Phys. Today* **65** 14
[14] Flensberg K 2010 *Phys. Rev.* B **82** 180516
[15] Kells G, Meidan D and Brouwer P W 2012 *Phys. Rev.* B **85** 060507
[16] Tewari S, Stanescu T D, Sau J D and Das Sarma S 2012 *Phys. Rev.* B **86** 024504
[17] Pientka F, Kells G, Romito A, Brouwer P W and von Oppen F 2012 arXiv:1206.0723
[18] Liu J, Potter A C, Law K T and Lee P A 2012 arXiv:1206.1276
[19] Slevin K, Pichard J-L and Mello P A 1996 *J. Phys.* I **6** 529
[20] Altland A and Zirnbauer M R 1997 *Phys. Rev.* B **55** 1142
[21] Rodríguez-Pérez S, Duarte-Filho G C and Macêdo A M S 2010 *Phys. Rev.* B **82** 115453
[22] Ivanov D A 2002 *J. Math. Phys.* **43** 126
[23] Ioselevich P A, Ostrovsky P M and Feigel'man M V 2012 *Phys. Rev.* B **86** 035441
[24] Bagrets D and Altland A 2012 arXiv:1206.0434
[25] Ryu S, Schnyder A, Furusaki A and Ludwig A 2010 *New J. Phys.* **12** 065010
[26] Tewari S and Sau J D 2012 *Phys. Rev. Lett.* **109** 150408
[27] Beenakker C W J, Dahlhaus J P, Wimmer M and Akhmerov A R 2011 *Phys. Rev.* B **83** 085413
[28] Diez M, Dahlhaus J P, Wimmer M and Beenakker C W J 2012 *Phys. Rev.* B **86** 094501
[29] Béri B 2009 *Phys. Rev.* B **79** 245315
[30] Wimmer M, Akhmerov A R, Dahlhaus J P and Beenakker C W J 2011 arXiv:1101.5795
[31] Whitney R S and Jacquod Ph 2009 *Phys. Rev. Lett.* **103** 247002
[32] Engl T, Kuipers J and Richter K 2011 *Phys. Rev.* B **83** 205414
[33] Akhmerov A R, Dahlhaus J P, Hassler F, Wimmer M and Beenakker C W J 2011 *Phys. Rev. Lett.* **106** 057001

[34] Pikulin D I and Nazarov Y V 2011 *JETP Lett.* **94** 693
[35] Wimmer M, Akhmerov A R, Dahlhaus J P and Beenakker C W J 2011 *New J. Phys.* **13** 053016
[36] Forrester P J 2010 *Log-Gases and Random Matrices* (Princeton, NJ: Princeton University Press)
[37] Dyson F J 1962 *J. Math. Phys.* **3** 1191
[38] Girko V L 1985 *Ukr. Mat. Zh.* **37** 568
Girko V L 1985 *Ukr. Math. J.* **37** 457 (Engl. transl.)
[39] Dyson F J 1972 *J. Math. Phys.* **13** 90